Voltage Stability Assessment of Grid Connected PV Systems With FACTS Devices

Melat Abdullah
University of Duhok
Lokman Hassan (lokman.hadi@uod.ac)
University of Duhok
M. Moghavvemi
University of Malaya

Research Article

Keywords: Power system stability, Voltage stability assessment, SPVGs, FACTS devices

Posted Date: December 2nd, 2021

DOI: https://doi.org/10.21203/rs.3.rs-1119382/v1

Voltage Stability Assessment of Grid Connected PV Systems with FACTS Devices

Melat K. Abdullah [1], Lokman H. Hassan [1, *], M. Moghavvemi [2,3]

1 Department of Electrical and Computer Engineering, University of Duhok, Duhok, Kurdistan Region, Iraq; lokman.hadi@uod.ac

2 Centre for Research in Applied Electronics (CRAE), Faculty of Engineering, University of Malaya, 50603 Kuala Lumpur, Malaysia; mahmoud@um.edu.my

3 University of Science and Culture, Tehran Iran

* Correspondence: lokman.hadi@uod.ac; +9647504739483

Abstract

Three static techniques (i.e., Power flow, Continuation Power Flow (CPF), and the Q-V curve) were used to assess the voltage stability of the power grid with a Solar Photovoltaic Generator (SPVG) and FACTS devices under nominal and heavy loading conditions. A static model is proposed for the power system that includes conventional power generation units and SPVGs with FACTS devices. Two models of SPVG were used (i.e., PV model and PQ model) to elucidate the effect of the SPVGs on the voltage stability under various operating conditions. The best location for FACTS devices was obtained under nominal and heavy load conditions using static techniques. The series and shunt FACTS devices under nominal and heavy loading conditions were compared using the abovementioned static techniques. The interaction between SPVGs and FACTS devices is detailed in this paper. The proposed approach was tested on the New England 39-bus standard test system, and the results confirmed the effectiveness of the proposed method under various operating conditions.

Keywords: Power system stability, Voltage stability assessment, SPVGs, FACTS devices.

1. Introduction

Voltage stability is the capability of a power grid at a specified initial operating condition to maintain steady voltages at all buses of the network under a disturbance. Voltage instability results in very low voltages in essential parts of the network, culminating in partial or total blackout, known as voltage collapse [1, 2].

Renewable energy sources, such as Solar Photovoltaic Generators (SPVGs), play an essential role in providing clean energy and ensuring adequate energy supply. SPVGs can also be used to inject reactive power into the grid. However, an SPVG in a network can cause system/voltage instability [3, 4], which makes it imperative that voltage stability be accounted for when connecting SPVG generators to the grid.

Dynamic and static are two approaches mentioned in the literature for investigating the voltage stability of grids. The dynamic analysis techniques were used in [5, 6] to confirm that the photovoltaic system can boost the system's power requirements. Hassan et al. [7] conducted a complete dynamic study of voltage stability impact on the IEEE 69-bus and 118-bus distribution grids with SPVGs. In [8], the long-term voltage stability of the network was improved after combining SPVG and Nordic-32 bus network using the time-domain simulation. However, dynamic analysis methods are time-consuming and are computationally intensive.

Static techniques are regularly used to investigate voltage stability due to their simplicity and reasonable accuracy [9]. In [10], the static characteristics of the SPVG emerging in a power grid were investigated using only the power flow technique. The SPVG's performance on voltage stability was modeled in [11] and [12] using a 14-bus with three generators test system and the Ontario test system as case studies, respectively. Both investigations utilized only the Continuation Power Flow (CPF) method. The presence of SPVG improved system stability by increasing the loadability boundary. The CPF method used in [13] analyzed the voltage stability of grid-connected SPVG power systems

under heavy load conditions. The Q-V curve method was used by Wang et al. [14] to elucidate the impact of the SPVG on the static voltage stability of China's Qinghai network, while [15] determined the effects of the SPVG on voltage stability boundary in an islanded microgrid using the P-V curve method. It is clear from the literature that the impact of the SPVG on voltage stability was investigated using only one of the static techniques.

The implementation of FACTS devices into the grid provided a significant opportunity to modify alternating current (AC) transmission, boost or decrease the power flow in certain buses, and respond immediately to instability issues [16]. In addition, the introduction of the FACTS device into the power grid improves its stability [17].

Anbarasan and Sanavullah [18] proposed using the CPF method to examine the grid in normal and heavy loadings settings. A Static Synchronous Compensator (STATCOM) was installed at the weakest bus in the network. It was pointed out that the voltage magnitude of the bus improved as long as the reactive power support was connected to the weakest bus. Finally, the V-Q sensitivity method was proposed by Prabhakar and Kumar [19] to highlight the impacts of High-Voltage Direct Current (HVDC), Static Var Compensator (SVC), Thyristor-Controlled Series Capacitor (TCSC), and Static Synchronous Compensator (STATCOM) on voltage stability.

In [20], an adaptive evolutionary algorithm used the automatic distribution of FACTS devices and variable tuning to improve voltage stability. [21] modeled the Static Synchronous Series Compensator (SSSC) to improve the system's voltage stability. A controllability index was proposed by Kumar et al. [22] to determine the optimal location of three types of FACTS devices for damping the inter-area mode of oscillations. Dynamic methods were used in [21] and [22].

This paper details a study conducted to highlight the impacts of SPVG and FACTS devices in enhancing the voltage stability of power systems using three static techniques (i.e., power flow, Q-V curve, and CPF). Two models of SPVG were used (i.e., PV-model and PQ-model) to demonstrate the effect of SPVGs on voltage stability under various operating conditions. The optimum location

for FACTS devices was determined under nominal and heavy load conditions. The series and shunt FACTS devices under both loading conditions were also compared. The intercommunication between SPVGs and FACTS devices is detailed in this paper. The results confirmed the effectiveness of the suggested approach when tested on the New England 39-bus standard test system under various operating conditions.

2. Modelling of solar photovoltaic generations with FACTS devices

This section detail the modeling of SPVGs with FACTS devices.

2.1 Modelling of the SPVGs

Figure 1 demonstrates the characteristic structure of a grid connected to a photovoltaic generator.

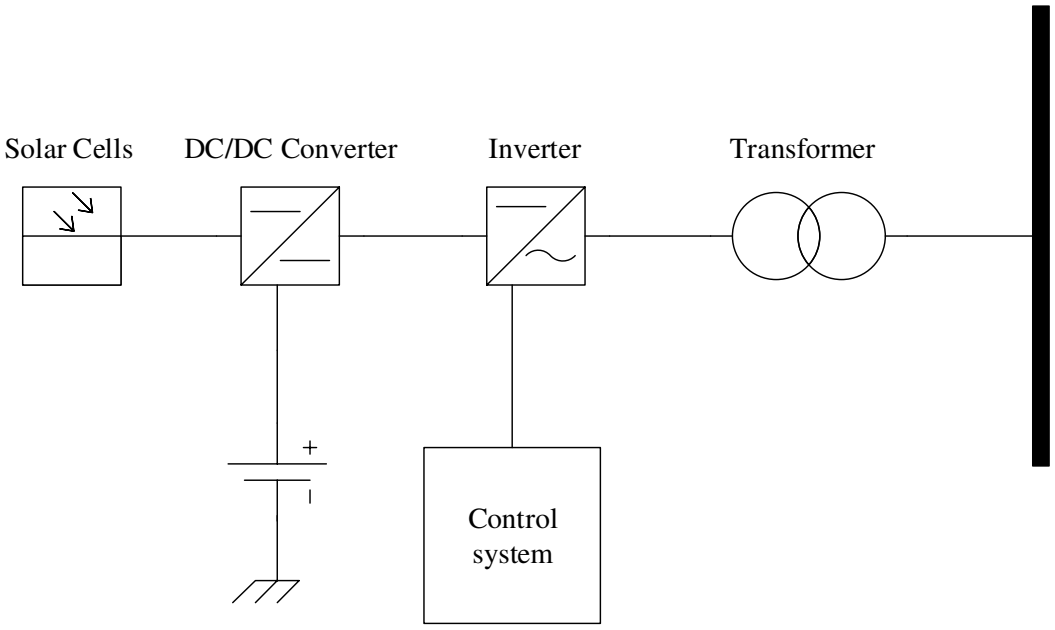

Figure 1. Structure of a grid-connected SPVG.

In this paper, two SPVG models were considered:

- PQ model when the active and reactive powers are constant.

- PV model when the active power and voltage are constant.

The SPVG consists of photovoltaic arrays, a DC/DC converter, and an inverter. The outputs of the inverter are [5]:

$$i_d = \frac{1}{1 + sT_p} i_{d\,s} \tag{1}$$

$$i_q = \frac{1}{1 + sT_q} i_{q\,s} \tag{2}$$

where i_d , i_q are the output currents of the inverter, T_p , T_q are the steady-state gains, and $i_{d\,s}$, $i_{q\,s}$ are the currents set-point.

The set-point currents can be calculated based on the selected active and reactive powers using the equation below:

$$\begin{bmatrix} i_{d\,s} \\ i_{q\,s} \end{bmatrix} = \begin{bmatrix} v_d & v_q \\ v_q & -v_d \end{bmatrix}^{-1} \begin{bmatrix} P \\ Q \end{bmatrix} \tag{3}$$

where v_d and v_q are the output voltages of the inverter.

The PV model can be obtained by adding a voltage regulator to the PQ model. In the PV model, the value of the reactive power reference is calculated based on the value of the actual and set-point voltage via the PI controller using the equation below:

$$\mathrm{Q} = (k_v + k_i s)(v_{dc} - v_{dc\,ref}) \tag{4}$$

where k_v and k_i are the voltage PI controller gains.

2.2 Modeling of FACTS devices

This work used classes of FACTS controllers (i.e., SVC, STATCOM, and TCSC).

A. Static Var Componsator (SVC)

SVC as shunt FACTS device offers dynamically flexible shunt impedance for controlling the bus voltage. Figure 2 shows the SVC model used in this work [23].

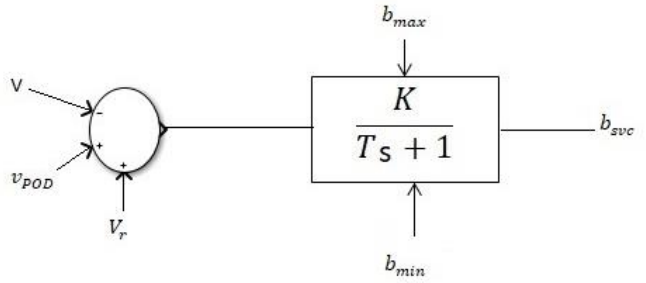

Figure. 2 SVC model.

The SVC's role in a system is to recompense the required amount of reactive power by generating reactive power at the connected bus. The total susceptance, $\hat{b}_{svc}$, is given by [23]:

$$\hat{b}_{svc} = (K(V_r + v_{POD} - V) - b_{svc})/T \tag{5}$$

Then, the reactive power generated by the SVC is:

$$Q = b_{svc}V^2 \tag{6}$$

where K is the gain, V_r is the voltage reference, v_{POD} is the voltage of the power oscillation damping, and T is the time constant.

B. Static Synchronous Compensator (STATCOM)

STATCOM is similar to SVC in providing shunt compensation, but it uses the voltage source converter. ~~Therefore, it combines a very high content of power electronics.~~ The implemented STATCOM model is a current booster model, and the STATCOM current is kept in quadrature with the voltage of the bus so that only reactive power is swapped between the STATCOM and AC system. Figure 3 shows the STATCOM model [23].

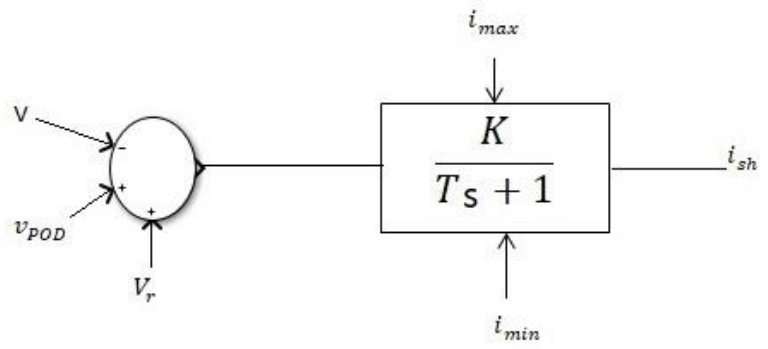

Figure 3. STATCOM model.

The equations of the current and reactive power generated by the STATCOM are:

$$\hat{\imath}_{sh} = (K(V_r + v_{POD} - V) - i_{sh})/T \tag{7}$$

$$Q = i_{sh}V \tag{8}$$

C. Thyristor-Controlled Series Capacitor (TCSC)

The model of a TCSC connected between bus k and bus m can be expressed as:

$$P_{km} = V_k V_m (Y_k + B)\sin(\theta_k - \theta_m) = -P_{mk} \tag{9}$$

$$Q_{km} = V_k^2 (Y_k + B) - V_k V_m (Y_k + B)\cos(\theta_k - \theta_m) \tag{10}$$

where k and m are the sending and receiving bus indices, respectively, and Y_k is the line admittance.

The TCSC model is shown in Figure 4 [23].

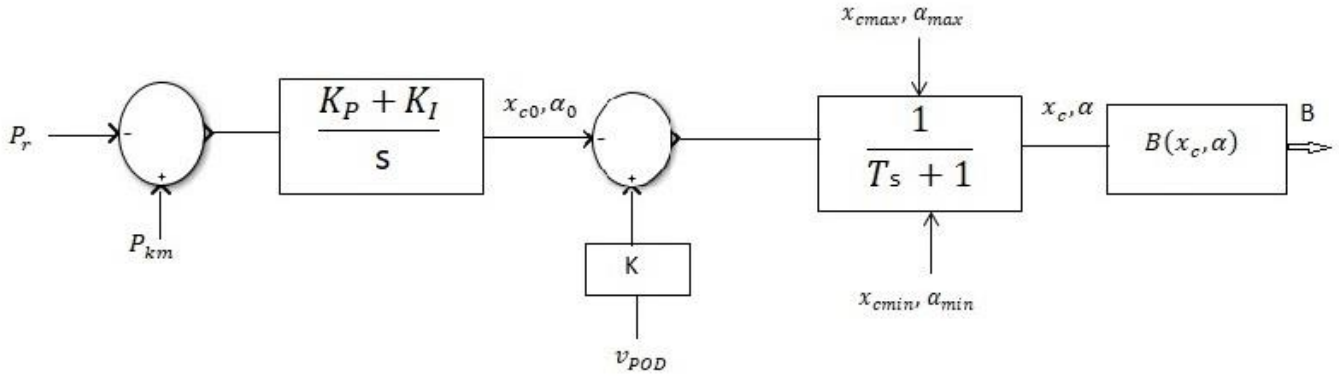

Figure 4. TCSC model.

The state equation of the TCSC is:

$$\vec{x}_1 = (\{x_{c0}, \alpha_0\} + K - x_1)/T \tag{11}$$

$$\vec{x}_2 = K_I(P_{km} - P_r) \tag{12}$$

$$\{x_{c0}, \alpha_0\} = K_p(P_{km} - P_r) + x_2 \tag{13}$$

where K_p and K_I are the proportional gain and the integral gain of the PI controller, respectively, x_c is the reactance, K is the gain of the stabilizing signal, and α_0 is the firing angle.

The state variable $x_1 = \{x_{c0}, \alpha_0\}$ depends on the TCSC model, and the PI controller is enabled during the constant power flow operation. The output signal is the series susceptance B of the TCSC and can be defined as:

$$B(x_c) = -\frac{x_c/x_m}{x_{km}(1-\frac{x_c}{x_m})} \tag{14}$$

The TCSC is molded as a constant capacitive reactance via the power flow analysis, which adjusts the line reactance, x_{km} , to:

$$\vec{x}_{km} = (1-c)x_{km} \tag{15}$$

where c is the percentage of series compensation.

3. Voltage stability analysis

This section describes the three static analysis techniques for voltage stability assessment. These techniques (power flow, Q-V cure, and continuous power flow) were used to measure the stability of the grid's voltage under various conditions.

3.1 Power flow analysis

The power industry depends on power flow to assess the voltage stability. The power flow analysis can calculate the power flow via a transmission line and voltage for buses or specific terminals. The system equations in terms of the bus admittance matrix can be written as [1]:

$$\vec{I}_b = \sum_{m=1}^{n} \vec{Y}_{bm}\ \vec{V}_m \tag{16}$$

where Y is admittance, b is bus number, and n is the number of buses.

The current at any bus is related to active power, reactive power, and voltage via:

$$\vec{I}_b = \frac{P_b - jQ_b}{\overrightarrow{V^*}_b} \tag{17}$$

where P is the active power and Q is the reactive power.

Then:

$$P_b + JQ_b = \vec{V}_b \sum_{m=1}^{n} (G_{bm} - JB_{bm}) \overrightarrow{V^*}_m \tag{18}$$

where G is conductance, B is susceptance, and $Y = G \pm jB$.

Then, the active and reactive powers at each bus are functions of voltage magnitude, making the phase angle:

$$P_b = V_b \sum_{m=1}^{n} (G_{bm} V_m \cos\theta_{bm} + B_{bm} V_m \sin\theta_{bm}) \tag{19}$$

$$Q_b = V_b \sum_{m=1}^{n} (G_{bm} V_m \sin\theta_{bm} - B_{bm} V_m \cos\theta_{bm}) \tag{20}$$

where θ_{bm} is the phase from bus to bus and equal to $\theta_b - \theta_m$.

3.2 Q–V modal analysis

Voltage is entirely associated with reactive power by assuming real power at every operating point is constant. Voltage stability can then be calculated via the incremental relation between reactive power and voltage [24]. The reduced Jacobian matrix becomes:

$$\Delta Q = J \Delta V \tag{21}$$

Furthermore, the Jacobian matrix can be factored as:

$$J = x \Lambda^{-1} \eta \tag{22}$$

where x is the suitable eigenvector matrix of the Jacobian matrix, Λ is the diagonal eigenvector matrix of the Jacobian matrix, and η is the left eigenvector matrix of the Jacobian matrix.

The variation of voltage against reactive power is:

$$\Delta V = x \Lambda^{-1} \eta \Delta Q \tag{23}$$

$$\Delta V = \sum_i (x_i \eta_i / \lambda_i) \Delta Q \tag{24}$$

where x_i is the ith column of the right eigenvalue of the Jacobian matrix, η_i is the ith row of the left eigenvalue of the Jacobian matrix, and λ_i is the i[th] eigenvalue of the Jacobian matrix obtained from the diagonal matrix(Λ^{-1}).

The voltage deviation for the *i*-th mode is:

$$V_i = \frac{1}{\lambda_i} q_i \tag{25}$$

Eigenvalues of the Jacobian matrix can serve as an indicator of the system's voltage stability. The grid is stable when all the eigenvalues are positive, and the grid is unstable when the minimum eigenvalue is equal to or less than zero. Therefore, the lower the positive eigenvalue, the closer the system is to voltage instability. The V–Q sensitivity at b bus is:

$$\frac{\partial V_b}{\partial Q_b} = \sum_i \frac{x_{bi}\, \eta_{bi}}{\lambda_i} \tag{26}$$

A negative Q-V sensitivity means that the grid is unstable. This implies that lower sensitivity means a more stable grid. The participation factor can be used to determine the relationship between the system buses and each eigenvalue, per the equation below:

$$P_{bi} = x_{bi}\, \eta_{bi} \tag{27}$$

3.3 Continuous power flow analysis

The continuation technique is a calculated path-following calculation procedure used to calculate nonlinear equations for the system [25]. From Newton-Raphson's method, load flow equations can be driven by introducing a load parameter into equations (19) and (20).

Let λ be the load factor, then:

$$P_{Lb} = P_{L0} + \lambda(R_{Lb} S_{base}\ cos\,\theta_b) \tag{28}$$

$$Q_{Lb} = Q_{L0} + \lambda(R_{Lb} S_{base}\ sin\,\theta_b) \tag{29}$$

where P_{L0} and Q_{L0} are nominal active and reactive load at bus b, R_{Lb} is a multiplier to show the load change at bus b as load factor (λ) changes, and S_{base} is a given amount of apparent power selected to provide a suitable value of λ.

The equations of power flow become:

$$F(\theta,\ \nu,\lambda) = 0 \tag{30}$$

where θ represents the vector of bus voltage angles and ν represents the vector of bus voltage magnitudes.

The active power generation term is adjusted to be:

$$P_{Gb} = P_{G0}(1 + \lambda R_{Gb}) \tag{31}$$

where P_{Gb} is the active power generation at bus *b,* P_{G0} is the initial value of active power generation, and R_{Gb} is the constant of varying rates in the generation to resolve the problem.

A linear estimate technique was utilized by selecting a suitable step size in a direction tangent to the resolution path. Then, (30) becomes:

$$F_\theta d\theta + F_\nu d\,\nu + F_\lambda d\lambda = [F_\theta\ F_\nu\ F_\lambda]\begin{bmatrix} d\theta \\ d\,\mathrm{v} \\ d\lambda \end{bmatrix} = 0 \tag{32}$$

After adding λ to the load flow equations, an additional equation is required to solve (32). This will be obtained by assuming one of the tangent vector components equal to +1 or -1, known as the continuation parameter.

$$\begin{bmatrix} F_\theta\ F_\nu F_\lambda \\ e_b \end{bmatrix}\begin{bmatrix} d\theta \\ d\,\mathrm{v} \\ d\lambda \end{bmatrix} = \begin{bmatrix} 0 \\ \pm 1 \end{bmatrix} \tag{33}$$

where e_b is the suitable row vector with entire elements equal to zero, excluding the b^{th} element equals 1.

First, λ is selected as the continuation parameter. Then, as the process is continued, the state variable with the highest amount of change is set as the continuation parameter because of the nature of parameterization. The tangent vector is obtained by solving (33), and the prediction is:

$$\begin{bmatrix} \theta \\ \mathrm{v} \\ \lambda \end{bmatrix}^{p+1} = \begin{bmatrix} \theta \\ \mathrm{v} \\ \lambda \end{bmatrix}^{p} + \sigma \begin{bmatrix} d\theta \\ d\,\mathrm{v} \\ d\lambda \end{bmatrix} \tag{34}$$

where the next step is designated by $p + 1$, and the step size σ is selected, so the estimated solution is within the radius of the corrector convergence.

The predicted result is adjusted via local parameterization. Equation (33) is improved using an equation that identifies the amount of state variable, selected as:

$$\begin{bmatrix} F(\theta, \mathrm{v}, \lambda) \\ x_b - \eta \end{bmatrix} = 0 \tag{39}$$

where x_b is state variable selected as continuation parameter and η is the predicted value of the state variable.

4. Results and Discussions

The New England 39-bus system was used to test the system. The single-line diagram of the system is shown in the Appendix. The study was carried out using Power System Analysis Toolbox (PSAT), a MATLAB-based toolbox for power system studies.

4.1 The weakest bus

Power flow and the Q-V curve were used for nominal conditions, and continuous power flow with the Q-V curve was used for heavy load conditions to identify the weakest buses of the system. The total power system losses were calculated for both conditions.

4.1.1 Nominal load condition

Table 1 shows the three weakest buses based on the power flow results.

Table 1. Power flow result.

Bus	V p.u.	Phase rad.	P_g p.u.	Q_g p.u.	P_L p.u.	Q_L p.u.
Bus 32	0.93491	-0.11367	0	0	0.075	0.88
Bus 17	0.94407	-0.18854	0	0	2.338	0.84
Bus 18	0.94479	-0.19837	0	0	5.220	1.76

The weakest buses are bus 32 with voltage 0.93491 pu, followed by buses 17 and 18 with voltages 0.94407 pu and 0.94479 pu, respectively.

The eigenvalue of each bus was calculated using the Q-V curve technique and listed in Table 2.

Table 2. The eigenvalue of weakest buses.

Bus	Eigenvalue
Bus 32	38
Bus 17	290
Bus 18	343

The results confirmed that bus 32 is the weakest bus of the system because it has the lowest eigenvalue of 38.

4.1.2 Heavy load condition

Table 3 shows the ten weakest buses per the CPF results.

Table 3. CPF results.

Bus	V p.u.	Phase rad.	P_g p.u.	Q_g p.u.	P_L p.u.	Q_L p.u.
Bus 17	0.58128	-0.84679	0	0	4.9133	1.7653
Bus 18	0.58496	-0.90244	0	0	10.9698	3.6986
Bus 32	0.58693	-0.50466	0	0	0.15761	1.8493

Under heavy load conditions, the weakest bus is bus 17 with voltage 0.58128 pu, bus 18 with a voltage of 0.58496 pu, and bus 32 with a voltage of 0.58693.

The eigenvalue of each bus was calculated and listed in Table 4.

Table 4. The eigenvalue of weakest buses at maximum load.

Bus	Eigenvalue
Bus 32	23
Bus 17	182
Bus 18	186

The system becomes unstable at heavy load conditions because one of the eigenvalues has a negative sign. For example, the eigenvalue 16 linked to bus 17 is equal to -0.77524.

4.2 The optimum location of FACTS devices

The optimum location for the FACTS devices is at the weakest bus [26]. The previous section identified buses 32 and 17 as the weakest ones under nominal and heavy load conditions. This section details the optimum location for installing the SVC device obtained using the proposed techniques.

4.2.1 SVC at bus 32

The power flow technique was applied under nominal load conditions, and the calculated results are listed in Table 5.

Table 5. Power flow results when SVC at bus 32.

Bus	V p.u.	Phase rad.	P_g p.u.	Q_g p.u.	P_L p.u.	Q_L p.u.
Bus17	0.95686	-0.18508	0	0	2.338	0.84
Bus18	0.95714	-0.19462	0	0	5.22	1.76
Bus32	1	-0.1146	0	2.025	0.075	0.88

After adding the SVC at bus 32, its voltage increased to 1 pu, bus 17's voltage increased to 0.95686 pu, and bus 18's voltage increased to 0.95714 pu. The improvement was due to the SVC consisting of reactive power amounting to 2.025 pu at bus 32.

The continuation power flow technique was applied under heavy load conditions, and the results are listed in Table 6.

Table 6. The results of the continuation power flow after adding SVC at bus 32.

Bus	V p.u.	Phase rad.	P_g p.u.	Q_g p.u.	P_L p.u.	Q_L p.u.
Bus17	0.60294	-0.81322	0	0	4.9565	1.7808
Bus18	0.60617	-0.86555	0	0	11.0663	3.7312
Bus32	0.62346	-0.4893	0	0	0.159	1.4769

After installing the SVC at bus 32, the voltage of bus 17 increased to 0.60294 pu, the voltage of bus 18 increased to 0.60617 pu, and the voltage of bus 32 increased to 0.62346.

The Q-V curve technique was used to check the system's stability, and the results show that there is no negative eigenvalue, which means that the system remains stable at heavy load conditions from the addition of SVC at bus 32.

4.2.1 SVC at bus 17

The power flow technique was applied under nominal load conditions, and the results are listed in Table 7.

Table 7. The results of power flow after adding SVC at bus 17.

Bus	V p.u.	Phase rad.	P_g p.u.	Q_g p.u.	P_L p.u.	Q_L p.u.
Bus17	1	-0.1808	0	3.9047	2.338	0.84
Bus18	0.99277	-0.18912	0	0	5.22	1.76
Bus32	0.95925	-0.10871	0	0	0.075	0.88

After adding SVC at bus 17, its voltage increased to 0.95925 pu, bus 17’s voltage increased to 1 pu, and bus 18’s voltage increased to 0.99277 pu, and the SVC’s composed reactive power amounted to 3.9047 pu at bus 17.

The continuation power flow technique was applied under heavy load conditions, and the results are listed in Table 8.

Table 8. The results of continuation power flow after adding SVC at bus 17.

Bus	V p.u.	Phase rad.	P_g p.u.	Q_g p.u.	P_L p.u.	Q_L p.u.

Bus17	0.59477	-0.83479	0	0	4.9499	1.4246
Bus18	0.59718	-0.88864	0	0	11.0515	3.7262
Bus32	0.59329	-0.4993	0	0	0.15879	1.8631

After adding the SVC at bus 17, bus 17's voltage increased to 0.59477 pu, bus 18's voltage increased to 0.59718 pu, and bus 32's voltage increased to 0.59329 pu.

The system becomes unstable at heavy load conditions using the Q-V curve technique because one eigenvalue is negative. For example, the eigenvalue 16 related to bus 17 is -0.95852.

From the results, it can be surmised that bus 17 is the optimal location for SVC under nominal load conditions for improving bus voltage. However, heavy load conditions connecting SVC to bus 32 resulted in better values than bus 17, where the system became unstable.

4.3 39-Bus System with SPVGs

This section details the PQ-model and PV-model of SPVG used to determine voltage stability. First, these models were tested at different load conditions, and the results were compared; then, the SVC was used to improve the voltage stability of the system via both models of SPVG. Finally, the generator at bus 10 was replaced by an SPVG using both models as it is the smallest conventional generator capacity in the network.

4.3.1 SPVG PQ-model

The power flow technique was applied to the system at nominal conditions, and the results are listed in Table 9.

Table 9. Power flow results when SPVG PQ-model is connected at bus 10.

Bus	V p.u.	Phase rad.	P_g p.u.	Q_g p.u.	P_L p.u.	Q_L p.u.
Bus17	0.94407	-0.18854	0	0	2.338	0.84
Bus18	0.94479	-0.19837	0	0	5.22	1.76
Bus32	0.93491	-0.11367	0	0	0.075	0.88

It can be seen that bus 32 is the weakest bus, with a voltage of 0.93491 pu, bus 17, with a voltage of 0.94407 pu, and bus 18, with a voltage of 0.94479 pu. The results are similar to those obtained when the ordinary generator is connected to bus 10. Therefore, it can be surmised that the results are unaffected when the standard generator is replaced with the SPVG PQ model.

The eigenvalue of each bus was calculated using the Q-V curve technique and listed in Table 10 .

Table 10. The eigenvalue of weakest buses with SPVG PQ-model.

Bus	Eigenvalue
Bus 32	42
Bus 17	308
Bus 18	312

After adding the SPVG PQ-model at bus 10, the eigenvalues increased, and bus 32 with an eigenvalue of 42 is identified as the weakest bus. Table 11 shows the results of the continuation power flow when the system is heavily loaded.

Table 11. Continuation power flow results with SPVG PQ-model at bus 10.

Bus	V p.u.	Phase rad.	P_g p.u.	Q_g p.u.	P_L p.u.	Q_L p.u.
Bus17	0.59568	-0.8884	0	0	4.5939	1.6505
Bus18	0.59968	-0.94345	0	0	10.2567	3.4582
Bus32	0.60762	-0.58859	0	0	0.14737	1.7291

At heavy load conditions, the weakest bus is bus 17, with a voltage of 0.59568 pu, bus18, with a voltage of 0.59968 pu, and bus32, with a voltage of 0.60762. The results show that the voltage buses increased after adding the SPVG PQ model at bus 10.

The system becomes unstable at maximum load condition using the Q-V curve technique because one eigenvalue is negative. For example, the eigenvalue 17 related to bus 17 is -1.3587. Table 12 shows the eigenvalues of the weakest buses.

Table 12. The eigenvalues of the weakest buses with SPVG PQ-model at heavy load conditions.

Bus	Eigenvalue

Bus 32	25
Bus 17	187
Bus 18	192

4.3.2 SPVG PQ-model with SVC

SVC was connected to bus 32 to enhance voltage stability, which is the optimum location, per section 4.2.

The power flow was applied to the system installed with SPVG PQ-model and SVC, and the results are listed in Table 13.

Table 13. Power flow result of the system installed with SPVG PQ-model and SVC.

Bus	V p.u.	Phase rad.	P_g p.u.	Q_g p.u.	P_L p.u.	Q_L p.u.
Bus17	0.95686	-0.18508	0	0	2.338	0.84
Bus18	0.95714	-0.19462	0	0	5.22	1.76
Bus32	1	-0.1146	0	2.025	0.075	0.88

The voltage at bus 32 increased to 1 pu, bus 17's voltage increased to 0.95686 pu, and bus 18's voltage increased to 0.95714 pu after SVC was added to the system. The voltage increased because the SVC's composed reactive power of 2.025 pu at bus 32.

The continuation power flow was applied to the system under heavy load conditions, and the results are listed in Table 14.

Table 14. Continuation power flow results of the system installed with SPVG PQ-model and SVC.

Bus	V p.u.	Phase rad.	P_g p.u.	Q_g p.u.	P_L p.u.	Q_L p.u.
Bus17	0.61181	-0.86445	0	0	4.6308	1.6638

Bus18	0.61544	-0.91715	0	0	10.339	3.486
Bus32	0.63962	-0.57671	0	0	0.14855	1.3339

After adding the SVC at bus 32, bus 17's voltage increased to 0.61181 pu, bus 18's voltage increased 0.61544 pu, and bus 32's voltage increased to 0.63962 pu.

The system remains unstable at maximum load even after adding SVC at bus 32 using the Q-V curve technique because one eigenvalue is negative. For example, eigenvalue 17 related to bus 17 is -0.97003.

4.3.3 SPVG PV-model

Power flow was applied to the system at nominal load conditions, and the results are listed in Table 15.

Table 15**.** Power flow results with SPVG PV-model are connected at bus 10.

Bus	V p.u.	Phase rad.	P_g p.u.	Q_g p.u.	P_L p.u.	Q_L p.u.
Bus17	0.94407	-0.18854	0	0	2.338	0.84
Bus18	0.94479	-0.19837	0	0	5.22	1.76
Bus32	0.93491	-0.11367	0	0	0.075	0.88

The results show that the weakest bus is bus 32, with a voltage of 0.93491 pu, bus 17, with a voltage of 0.94407 pu, and bus 18, with a voltage of 0.94479 pu.

The eigenvalue of each bus was calculated using the Q-V curve technique and listed in Table 16.

Table 16. The eigenvalue of weakest buses of the system with SPVG PV-model.

Bus	Eigenvalue
Bus 32	42
Bus 17	308
Bus 18	312

The eigenvalues increased after connecting the SPVG PV-model at bus 10. The weakest bus is bus 32, with an eigenvalue of 42. The buses voltage and total losses of the system at nominal load conditions were unchanged after connecting the SPVG to the system.

The continuation power flow was applied to the system when it was heavily loaded, and the results are listed in Table 17.

Table 17. Continuation power flow of the system with SPVG PV-model.

Bus	V p.u.	Phase rad.	P_g p.u.	Q_g p.u.	P_L p.u.	Q_L p.u.
Bus17	0.61551	-0.87518	0	0	4.7261	1.698
Bus18	0.61925	-0.92807	0	0	10.552	3.5578
Bus32	0.62574	-0.58461	0	0	0.15161	1.7789

The results confirmed that the weakest bus is bus 17, with a voltage of 0.61551 pu, bus 18, with a voltage of 0.61925 pu, and bus 32, with a voltage of 0.62574. The voltages of the buses increased after using the SPVG PV model.

After the SPVG PQ model was used at bus 10, the buses' voltage increased ~0.015 pu for each bus, but when the SPVG PV model was connected at bus 10, the buses' voltage increased ~0.035 pu for each bus at heavy load conditions. Thus, the results confirmed that the SPVG PV model is more efficient than the SPVG PQ model in improving the system's buses voltage under heavy load conditions.

The system becomes unstable under heavy load conditions using the Q-V curve technique because one of the eigenvalues is negative. For example, the eigenvalue 18 related to bus 17 is -0.05095. Table 18 shows the eigenvalues of the weakest buses.

Table 18. Eigenvalues of weakest buses of the system with SPVG PV-model at heavy load condition.

Bus	Eigenvalue
Bus 32	26
Bus 17	193
Bus 18	198

The system with the SPVG PV model and the SPVG PQ mode is unstable under heavy load conditions.

4.3.4 SPVG PV-model with SVC

The power flow was applied to the system at nominal load condition, and the results are listed in

Table **19**.

When the SVC was connected to the weakest bus, the voltage at bus 32 increased to 1 pu, bus 17 to 0.95686 pu, and bus 18 to 0.95714 pu because the SVC injected 2.025 pu reactive power to the system at bus 32.

Table 19. Power flow results of the system with SPVG PV-model and SVC.

Bus	V p.u.	Phase rad.	P_g p.u.	Q_g p.u.	P_L p.u.	Q_L p.u.
Bus17	0.95686	-0.18508	0	0	2.338	0.84
Bus18	0.95714	-0.19462	0	0	5.22	1.76
Bus32	1	-0.1146	0	2.025	0.075	0.88

The continuation power flow was applied to the system at heavy load conditions, and the results are listed in Table 20.

Table 20. Continuous power flow results of the system with SPVG PV-model and SVC.

Bus	V p.u.	Phase rad.	P_g p.u.	Q_g p.u.	P_L p.u.	Q_L p.u.
Bus17	0.62733	-0.85951	0	0	4.7572	1.7092

Bus18	0.63077	-0.91084	0	0	10.6212	3.5811
Bus32	0.65464	-0.57763	0	0	0.1526	1.362

The voltages of buses 17, 18, and 32 increased to 0.62733 pu, 0.63077 pu, and 0.65464, respectively, after the SVC was installed at bus 39.

The system is stable under heavy load conditions applying the Q-V cure method because all eigenvalues are positive.

4.4 System with Shunt and Series FACTS Devices

Previous sections detail the SVC as a shunt FACTS device being used to improve the voltage stability of the system. This section describes the STATCOM as shunt FACTS device and TCSC as series FACTS device being used, and the results compared.

4.4.1 System with STATCOM

The power flow technique was applied to the system at nominal load conditions, and the results are listed in

Table **21**.

Table 21. Power flow result of the system with STATCOM installed.

Bus	V p.u.	Phase rad.	P_g p.u.	Q_g p.u.	P_L p.u.	Q_L p.u.
Bus17	0.95686	-0.18508	0	0	2.338	0.84
Bus18	0.95714	-0.19462	0	0	5.22	1.76
Bus32	1	-0.1146	0	2.025	0.075	0.88

When STATCOM was used, the voltages at bus 32, bus 17, and bus 18 increased to 1 pu, 0.95686 pu, and 0.95714 pu, respectively.

From the results, it can be surmised that there are no differences between the results obtained using SVC and those obtained using STATCOM at nominal load conditions.

The continuation power flow was applied to the system under heavy load conditions, and the results are listed in

Table **22**.

When STATCOM was installed, the voltages of buses 17, 18, and 32 increased to 0.61649 pu, 0.62005 pu, and 0.66152, respectively.

Table 22. Continuation power flow results of the system with STATCOM installed.

Bus	V p.u.	Phase rad.	P_g p.u.	Q_g p.u.	P_L p.u.	Q_L p.u.
Bus17	0.61649	-0.88635	0	0	4.7794	1.7172
Bus18	0.62005	-0.93974	0	0	10.6709	3.5978
Bus32	0.66152	-0.59682	0	2.00E-05	0.15332	1.0051

The system becomes unstable at maximum load conditions using the Q-V curve technique because one eigenvalue is negative. For example, the eigenvalue 17 related to bus 17 is -0.15514.

The results show that SVC is more efficient than STATCOM in terms of bus voltage and stability.

4.4.1 System with TCSC

The power flow technique was applied to the system when the load was nominal, and the results are listed in Table 23.

Table 23 Power flow results of the system with TCSC installed.

Bus	V p.u.	Phase rad.	P_g p.u.	Q_g p.u.	P_L p.u.	Q_L p.u.
Bus17	0.94392	-0.18857	0	0	2.338	0.84
Bus18	0.94465	-0.1984	0	0	5.22	1.76
Bus32	0.94231	-0.1141	0	0	0.075	0.88

After connecting the TCSC in series with lines 31-32, the voltages at buses 32, 17, and 18 increased to 0.94231 pu, 0.94392 pu, and 0.94465 pu, respectively.

The system with TCSC installed in lines 31-32 at nominal load conditions reported lower bus voltages than SVC and STATCOM.

The continuation power flow was applied at heavy load conditions, and the results are listed in Table 24.

Table 24. Continuation power flow of the system with TCSC installed.

Bus	V p.u.	Phase rad.	P_g p.u.	Q_g p.u.	P_L p.u.	Q_L p.u.
Bus17	0.62513	-0.85446	0	0	4.7133	1.6934
Bus18	0.62866	-0.9058	0	0	10.5232	3.5481
Bus32	0.55153	-0.58443	0	0	0.1512	1.774

The results show that the voltages of buses 17, 18, and 32 increased to 0.62513 pu, 0.62866 pu, and 0.55153 pu, respectively, after TCSC was installed in lines 31-32.

The system is stable under heavy load conditions applying the Q-V curve when TCSC is connected in series with lines 31-32.

The system with TCSC installed at heavy load conditions reported lower bus voltage than the system with SVC or STATCOM installed. The system with TCSC installed is stable at heavy load conditions, while the system with STATCOM installed is unstable.

5. Conclusion

This paper detailed the use of three static techniques (power flow, Q-V curve, and continuation power flow) to assess the voltage stability of a power grid. First, the weakest bus in the grid under nominal and heavy loading conditions was obtained using the New England 39-bus system as a test case. Buses 32 and 17 were identified as weakest buses under nominal load and heavy load conditions, respectively, and the system became unstable under heavy loading conditions. Second, FACTS devices were used to improve the voltage stability of the system. The optimum location of FACTS

devices was obtained using three static techniques under both loading conditions. It was concluded that bus 32 is the optimal location for SVC devices under heavy loading conditions. The voltage of the buses increased ~6.5% and ~3.6% at nominal load and heavy load conditions, respectively, when using FACTS devices.

PQ model and PV model for SPVG were used to assess the stability of voltage. First, these models were tested at different load conditions, and the results were compared. Then, the FACTS devices were used to improve the voltage stability of the system with the PQ-model and PV-model of SPVG. Finally, the generator at bus 10 was replaced by SPVGs, and the voltage stability of the system was enhanced after the addition of the SPVG to the system. The results showed that the SPVG PV model is more effective than the SPVG PQ model in improving the system's voltage stability, reporting an improvement of ~3%.

Finally, three types of FACTS devices (i.e., SVC, STATCO, M, and TCSC) were compared under nominal and heavy loading conditions using the abovementioned static techniques.

APPENDIX A

A single line diagram of the New England 39-bus system

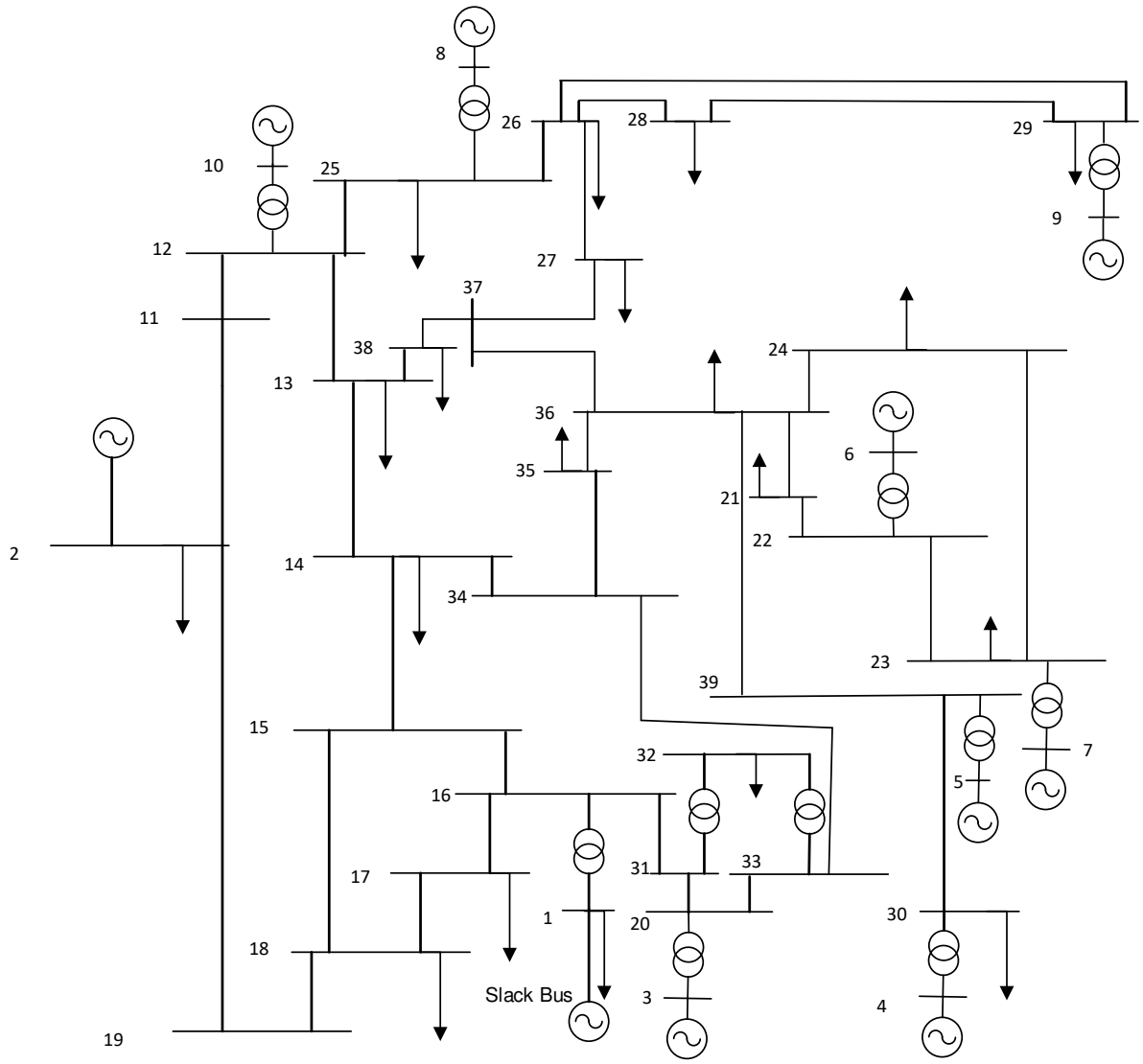

References

[1] M. J. Vahid-Pakdel, H. Seyedi, and B. Mohammadi-Ivatloo, "Enhancement of Power System Voltage Stability in Multi-Carrier Energy Systems," *International Journal of Electrical Power & Energy Systems,* vol. 99, pp. 344-354, 2018/07/01/ 2018.

[2] P. Kundur *et al.*, "Definition and Classification of Power System Stability IEEE/CIGRE Joint Task Force on Stability Terms And Definitions," *IEEE Transactions on Power Systems,* vol. 19, no. 3, pp. 1387-1401, 2004.

[3] A. Omole, "Voltage Stability Impact of Grid-Tied Photovoltaic Systems Utilizing Dynamic Reactive Power Control," Ph.D. Thesis, 2010.

[4] M. El-Shimy, A. Sharaf, H. Khairy, and G. Hashem, "Reduced-order modelling of solar-PV generators for small-signal stability assessment of power systems and estimation of maximum penetration levels," *IET Generation, Transmission & Distribution,* vol. 12, no. 8, pp. 1838-1847, 2018.

[5] S. S. Refaat, H. Abu-Rub, A. P. Sanfilippo, and A. Mohamed, "Impact of Grid-Tied Large-Scale Photovoltaic System on Dynamic Voltage Stability of Electric Power Grids," *IET Renewable Power Generation*, vol. 12, no. 2, pp. 157-164Available: https://digital-library.theiet.org/content/journals/10.1049/iet-rpg.2017.0219

[6] D. Noel, F. Sozinho, D. Wilson, and K. Hatipoglu, "Analysis of Large Scale Photovoltaic Power System Integration into the Existing Utility Grid Using PSAT," in *SoutheastCon 2016*, 2016, pp. 1-7.

[7] L. H. Hassan, "Impact of a PV Controller on Stability of Renewable Energy Based Large Distribution Systems " presented at the 3rd International conference on artificial intelligence, computer, electrical and electronics engineering (ICACEEE), Kuala Lmpur, Feb 9-10, 2017.

[8] E. Munkhchuluun and L. Meegahapola, "Impact of The Solar Photovoltaic (PV) Generation on Long-Term Voltage Stability of a Power Network," in *2017 IEEE Innovative Smart Grid Technologies - Asia (ISGT-Asia)*, 2017, pp. 1-6.

[9] L. H. Hassan, H. A. Mohamed, M. Moghavvemi, and S. Yang, "Contingency Monitoring and Voltage Collapse Estimation for Iraqi National Super Grid System," in *The 4th International Colloquium on Signal Processing and its Applications (CSPA) 2008* Kuala Lumpur, 2008, pp. 570- 574.

[10] Y.-B. Wang, C.-S. Wu, H. Liao, and H.-H. Xu, "Steady-State Model and Power Flow Analysis of Grid-Connected Photovoltaic Power System," in *2008 IEEE International Conference on Industrial Technology*, 2008, pp. 1-6.

[11] B. Tamimi, C. Cañizares, and K. Bhattacharya, "Modeling and Performance Analysis of Large Solar Photo-Voltaic Generation on Voltage Stability and Inter-Area Oscillations," in *2011 IEEE Power and Energy Society General Meeting*, 2011, pp. 1-6.

[12] B. Tamimi, C. Canizares, and K. Bhattacharya, "System Stability Impact of Large-Scale and Distributed Solar Photovoltaic Generation: The Case of Ontario, Canada," *IEEE Transactions on Sustainable Energy,* vol. 4, no. 3, pp. 680-688, 2013.

[13] W. Suampun, "Voltage Stability Analysis of Grid-connected Photovoltaic Power Systems Using CPFLOW," *Procedia Computer Science,* vol. 86, pp. 301-304, 2016/01/01/ 2016.

[14] D. Wang, X. Yuan, M. Zhao, and Y. Qian, "Impact of Large-Scale Photovoltaic Generation Integration Structure on Static Voltage Stability in China's Qinghai Province Network," *The Journal of Engineering,* vol. 2017, no. 13, pp. 671-675, 2017.

[15] R. L. Sinder, T. M. L. Assis, and G. N. Taranto, "Impact of Photovoltaic Systems on Voltage Stability in Islanded Distribution Networks," *The Journal of Engineering,* vol. 2019, no. 18, pp. 5023-5027, 2019.

[16] F. M. Albatsh, S. Mekhilef, S. Ahmad, H. Mokhlis, and M. A. Hassan, "Enhancing power transfer capability through flexible AC transmission system devices: a review," *Frontiers of Information Technology & Electronic Engineering,* vol. 16, no. 8, pp. 658-678, 2015/08/01 2015.

[17] F. H. Gandoman *et al.*, "Review of FACTS technologies and applications for power quality in smart grids with renewable energy systems," *Renewable and Sustainable Energy Reviews,* vol. 82, pp. 502-514, 2018/02/01/ 2018.

[18] A. Anbarasan and M. Y. Sanavullah, "VOLTAGE STABILITY IMPROVEMENT IN POWER SYSTEM BY USING STATCOM," 2012.

[19] P. Prabhakar and A. Kumar, "Voltage stability boundary and margin enhancement with FACTS and HVDC," *International Journal of Electrical Power & Energy Systems,* vol. 82, pp. 429-438, 2016/11/01/ 2016.

[20] S. d. Nascimento and M. M. Gouvêa, "Voltage Stability Enhancement in Power Systems with Automatic Facts Device Allocation," *Energy Procedia,* vol. 107, pp. 60-67, 2017/02/01/ 2017.

[21] D. A. Ingole and P. D. V. N. Gohokar, "Voltage Stability Improvement In Multi-bus System Using Static Synchronous Series Compensator," *Energy Procedia,* vol. 117, pp. 999-1006, 2017/06/01/ 2017.

[22] B. K. Kumar, S. N. Singh, and S. C. Srivastava, "Placement of FACTS controllers using modal controllability indices to damp out power system oscillations," *IET Generation, Transmission & Distribution*, vol. 1, no. 2, pp. 209-217Available: https://digital-library.theiet.org/content/journals/10.1049/iet-gtd_20050529

[23] F. Milano, *Power System Analysis Toolbox: Documentation for PSAT version 2.1.11*. Independently published, 2020.

[24] K. Z. Heetun, S. H. E. Abdel Aleem, and A. F. Zobaa, "Voltage Stability Analysis of Grid-Connected Wind Farms With FACTS: Static and Dynamic Analysis," *Energy and Policy Research,* vol. 3, no. 1, pp. 1-12, 2016/01/01 2016.

[25] A. D. Vasquez and U. T. Sousa, "Voltage Stability Analysis of Power Systems using the Continuation Method " presented at the THE 12th LATIN-AMERICAN CONGRESS ON ELECTRICITY GENERATION AND TRANSMISSION, Mar del Plata, Argentina, Nov 12-15, 2017.

[26] M. K. Jalboub, H. S. Rajamani, J. C. Readle, R. A. Abd-Alhameed, and A. M. Ihbal, "Weakest bus identification for optimal location for FACTS systems in multi-machine power network," *International Journal of Power and Energy Conversion,* vol. 3, no. 1-2, pp. 127-142, 2012.